Journal of Hepatocellular Carcinoma

Dovepress
Taylor & Francis Group

Open Access Full Text Article

ORIGINAL RESEARCH

Prognostic Nomogram for Hepatocellular Carcinoma Patients with High Systemic Immune-Inflammation Index: Validation in Surgical and Immunotherapy Cohorts and Exploration of Immune Microenvironment Mechanisms

Xinxin Wang[1,*], Zhe Hu[1,*], Jiaxuan Ding[1], Suyongde Zheng[2], Bangcheng Wei[3,4], Yang Zhou[1], Shuhong Wang[1]

[1]Department of Radiology, Harbin Medical University Cancer Hospital, Harbin, Heilongjiang, 150081, People's Republic of China; [2]Department of Nuclear Medicine, Harbin Medical University Cancer Hospital, Harbin, Heilongjiang, 150081, People's Republic of China; [3]Clinical Medical College, Jining Medical University, Jining, Shandong, 272067, People's Republic of China; [4]Department of Radiology, Affiliated Hospital of Jining Medical University, Jining, Shandong, 272007, People's Republic of China

*These authors contributed equally to this work

Correspondence: Shuhong Wang; Yang Zhou, Department of Radiology, Harbin Medical University Cancer Hospital, Harbin, Heilongjiang, 150081, People's Republic of China, Email wangshuhong3656@163.com; zhouyang094@126.com

Background: The systemic immune-inflammation index (SII) has emerged as a robust prognostic indicator in hepatocellular carcinoma (HCC). However, precise risk stratification for HCC patients with high preoperative inflammatory burden—a group typically associated with poor prognosis—remains a clinical challenge. This study aimed to develop and validate a multi-center radiomics-clinicopathologic nomogram to optimize individualized survival prediction for this specific subpopulation.

Methods: We conducted a multi-center retrospective study involving HCC patients with high preoperative SII from two medical centers. Patients were stratified into a training cohort, an external validation cohort, and an independent immunotherapy cohort to evaluate model generalizability. Radiomics features were extracted from preoperative imaging. A prognostic nomogram was constructed using multivariable Cox regression analysis, integrating the radiomics score (Rad-score), clinical factors (e.g. tumor diameter, AFP), and pathologic features. The model's performance was rigorously assessed via C-index, calibration curves, and Decision Curve Analysis (DCA). Furthermore, bulk transcriptomic analysis of our own patient samples was performed to elucidate the underlying immune microenvironment mechanisms associated with high SII.

Results: The integrative nomogram demonstrated superior predictive accuracy compared to traditional staging systems. In the training cohort, the C-index was 0.796, which remained robust in the external surgical validation cohort (0.775). DCA confirmed that the nomogram provided significant clinical net benefit across different therapeutic settings. Transcriptomic analysis revealed that high-risk patients were characterized by an immunosuppressive microenvironment, marked by the enrichment of pathways related to cytokine–cytokine receptor interaction and significant infiltration of regulatory T cells (Tregs).

Conclusion: We developed and validated a robust radiomics-clinicopathologic nomogram specifically for HCC patients with high inflammatory burden. This multi-center tool provides accurate risk stratification across both surgical and immunotherapy settings, potentially facilitating more personalized clinical decision-making.

Keywords: hepatocellular carcinoma, systemic immune-inflammation index, nomogram, recurrence-free survival, immunotherapy, transcriptomics

https://doi.org/10.2147/JHC.S588390
Received: 12 December 2025
Accepted: 18 March 2026
Published: 30 March 2026

Introduction

Primary Hepatocellular carcinoma (HCC) is one of the leading causes of cancer-related mortality worldwide, and its incidence has continued to rise in Asia and some Western countries in recent years.[1] Although surgical resection, as one of the curative treatment options, significantly improves long-term survival in early-stage patients, the postoperative recurrence rate remains high at 50%–70%, severely restricting prognostic improvement.[2,3] On the other hand, with the widespread use of immune checkpoint inhibitors (ICIs), immunotherapy has gradually become a key treatment modality for advanced and even some intermediate-to-early-stage HCC.[4,5] However, The therapeutic effect varies significantly among different immunoheterogeneous populations.[6–8] Therefore, risk stratification and individualized prognostic assessment for HCC patients with different inflammatory responses have become critical subjects in clinical and translational research.

In recent years, increasing evidence suggests that the host's systemic inflammation and immune status play a crucial role in the development, progression, and treatment response of HCC. Various inflammatory markers, such as the Neutrophil-to-Lymphocyte Ratio (NLR) and Platelet-to-Lymphocyte Ratio (PLR), have been widely utilized to predict patient outcomes by reflecting the balance between pro-tumor inflammation and anti-tumor immunity. However, compared to these traditional binary ratios, the Systemic Immune-Inflammation Index (SII)—calculated from peripheral blood platelet, neutrophil, and lymphocyte counts—offers a more comprehensive integration of three independent inflammatory pathways. By incorporating the platelet count, which is closely linked to tumor-associated angiogenesis and metastasis, SII provides a more robust reflection of the tumor-associated inflammatory response and immune capacity than NLR or PLR alone.[9,10] A high SII often suggests platelet-mediated angiogenesis, neutrophil-associated pro-tumor inflammation, and impaired anti-tumor immunity due to lymphopenia, thus correlating closely with adverse prognosis. Multiple studies have confirmed that SII serves as an independent predictor of overall survival (OS) and disease-free survival/recurrence-free survival (DFS/RFS), and has been incorporated into various risk prediction models or nomograms.[11,12]

Nevertheless, current research has several limitations. First, most studies focus on the overall population, with few models specifically tailored for the high-SII high-risk subpopulation, leading to insufficient predictive power for patients with a high inflammatory burden. Second, existing SII-based nomograms predominantly rely on traditional clinical variables, particularly Alpha-fetoprotein (AFP) and staging information, with limited integration of radiological non-invasive features, which hold irreplaceable value in revealing tumor biological behavior and patient prognosis. Third, although ICIs therapy is rapidly changing the landscape of HCC treatment, scarcely any studies have validated the generalization capability of SII-stratified nomograms in the immunotherapy population. Finally, the molecular mechanisms underlying the association between SII and prognosis remain incompletely understood, and transcriptomic studies could offer critical clues to its biological basis.

Based on this background, the present study proposes and validates a novel risk assessment strategy, integrating radiological and inflammatory immune markers, specifically for HCC patients with a high inflammatory burden.This study aims to establish a simple, robust, and clinically accessible prediction tool to achieve individualized risk assessment and optimize treatment decisions for HCC patients across different therapeutic settings.

Materials and Methods

Study Design and Patient Source

This was a multicenter retrospective cohort study. Patients were recruited from the Harbin Medical University Cancer Hospital (Jan 2015–Jun 2025) and the Affiliated Hospital of Jining Medical University (Jan 2020–Jun 2025). All patients were pathologically or radiologically confirmed with HCC. The study protocol adhered to the Declaration of Helsinki and was approved by the institutional ethics committee (Ethics Number: KY2024-33). All data were de-identified before analysis.

Inclusion Criteria

(1) Diagnosed with definite HCC; (2) Complete baseline preoperative peripheral blood routine and biochemical markers were available; (3) For the surgical cohort: received curative resection, pathological confirmation of negative margins,

and completed at least one follow-up; (4) For the immunotherapy cohort: received single-agent or combination ICIs therapy, and had radiological follow-up data to assess efficacy.

Exclusion Criteria

(1) Concurrent active malignancy; (2) Presence of severe infection or autoimmune disease; (3) Preoperative systemic anti-tumor treatment that prevented accurate reflection of the true blood profile; (4) Missing critical clinical or follow-up data.

The Harbin Medical University Cancer Hospital finally included a total of N_total = 669 patients, comprising N_surgery = 535 in the surgical cohort, and N_ICI = 134 in the immunotherapy cohort. The Affiliated Hospital of Jining Medical University finally included N_surgery = 114 patients in the surgical cohort. The patient inclusion and exclusion process is shown in Figure 1.

SII Calculation and Grouping

The formula for the SII is P × N / L (P is the platelet count in the complete blood count; N is the neutrophil count; L is the lymphocyte count).

The optimal cutoff value for surgical cohort patients was determined using maximally selected rank statistics (surv cutpoint method). Using this value as the boundary, patients were divided into low-SII and high-SII groups. Baseline clinical characteristics between the two groups were compared (Chi-square test or Fisher's exact test), and Kaplan–Meier curves for OS and RFS were plotted for the surgical cohort patients, with differences evaluated by the Log rank test.

Construction and Variable Selection of the Training-Test Cohort for High SII Population

Within the high-SII population, patients were randomly divided into a training cohort and a test cohort at a 7:3 ratio. The training cohort was used for variable selection and model construction, while the test cohort was used for independent test of model performance. Candidate variables included clinical indicators, radiological features, and biochemical markers. In the training cohort, univariate Cox proportional hazards regression analysis was first performed to screen variables with $P < 0.05$. These variables were then included in multivariate Cox regression. Finally, independent prognostic factors were identified, and their Hazard Ratios (HR) and 95% Confidence Intervals (CI) were calculated. Based on the regression coefficients from the multivariate Cox regression, a nomogram was constructed using the rms package in R language to predict 1-, 2-, and 3-year RFS.

Model Evaluation and Test

The following evaluations were performed in the training and test cohorts, respectively: Discriminative ability was assessed by calculating Harrell's C-index and the Area Under the Curve (AUC) of time-dependent Receiver Operating Characteristic (ROC) curves for 1, 2, and 3 years. Based on the median total score of the nomogram in the training set, high-SII patients were stratified into high-risk and low-risk groups. Kaplan–Meier curves were used to compare the difference in RFS (Log rank test). The model was migrated to the immunotherapy cohort, and the nomogram score for each patient was calculated to predict 1-, 2-, and 3-year PFS. The same median cutoff value was used to stratify risk groups, and survival curves were plotted to assess the model's generalization performance. To systematically compare the predictive performance of this study's nomogram with existing clinical staging systems, the AJCC 8th edition and BCLC staging systems were selected as references. Discriminative ability was assessed by calculating the Harrell's C-index and time-dependent ROC (1-, 2-, 3-year AUC) for each model in the training and test sets.

Transcriptomic Analysis

Transcriptomic analysis was performed on 67 high-SII surgical patients with RNA sequencing (RNA-seq) data. Patients were divided into high-risk and low-risk groups based on the median score calculated by the nomogram. Raw FASTQ files were quality-controlled to remove low-quality reads. The cleaned sequences were aligned to the reference genome (GRCh38) using HISAT2, and the raw read count matrix at the gene level was obtained using featureCounts.

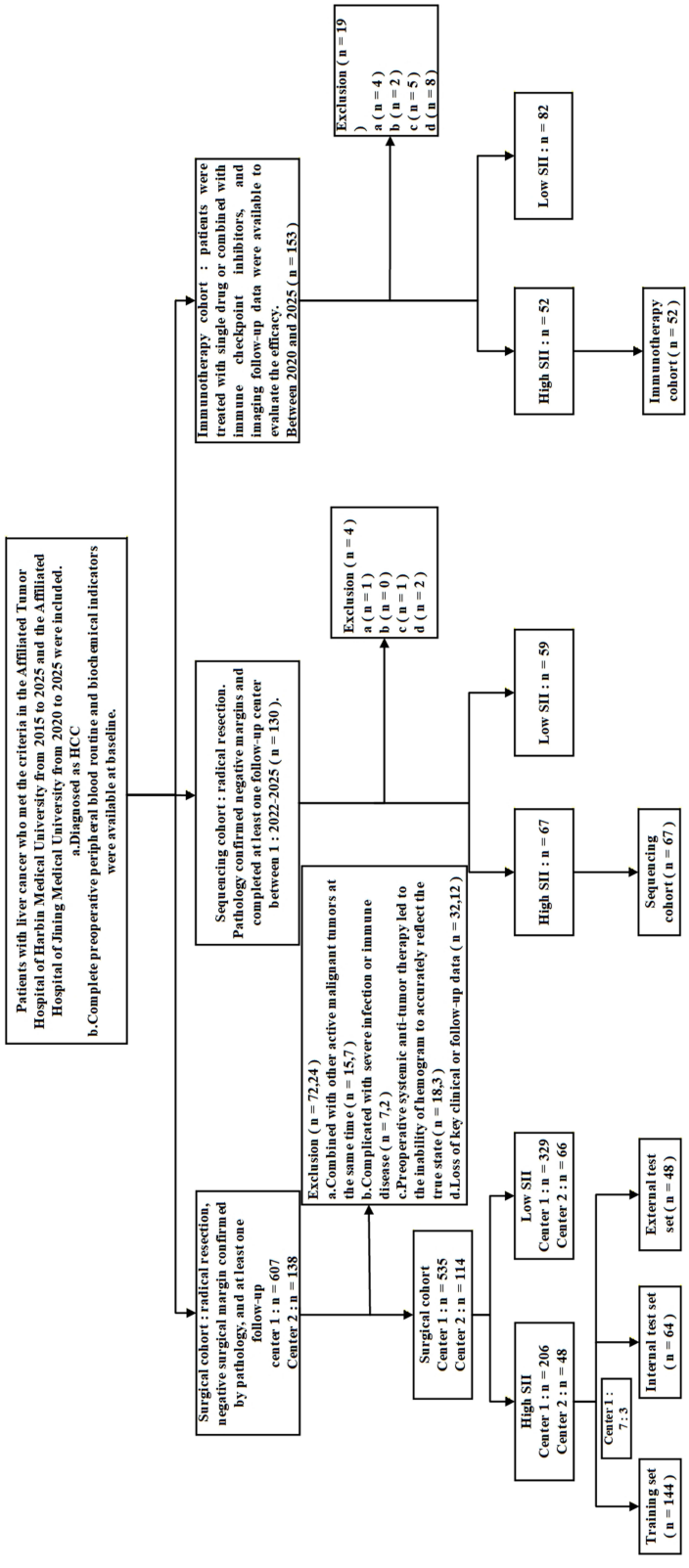

Figure 1 Standard diagram of patient 's admission.

Subsequently, the edgeR package was used for standardization (Trimmed Mean of M-values, TMM method), and the Transcripts Per Million (TPM) abundance for each gene was calculated for subsequent differential analysis and visualization. Differentially Expressed Genes (DEGs) analysis was performed using edgeR, with a threshold set at $\log_2FC > 1$ and False Discovery Rate (FDR) < 0.05. Several DEGs were identified between the high-risk and low-risk groups, and used for functional annotation and signal pathway enrichment analysis. Kyoto Encyclopedia of Genes and Genomes (KEGG) pathway enrichment analysis and Gene Ontology (GO) Biological Process (BP) enrichment analysis were performed based on the DEGs, using the clusterProfiler package to calculate enrichment significance (P.adjust < 0.05). CIBERSORT and quanTIseq algorithms were used to assess changes in the infiltration proportion of immune cell subpopulations in the tumor microenvironment. Using the oncoPredict package, the GDSC2 cell line expression profile and drug response matrix were used as the training set, and the drug sensitivity of each sample was predicted using calcPhenotype (empirical Bayes batch correction, low-variance gene filtering) from our cohort's expression data. Drug sensitivity (measured as $\ln(IC_{50})$ AUC, depending on the training label) was obtained and compared between the risk groups.

Statistical Analysis

Quantitative data are presented as mean ± Standard Deviation (SD) or median (Interquartile Range, IQR), and comparisons were made using the *t*-test or Mann–Whitney *U*-test. Categorical data are presented as frequency (%), and comparisons were made using the Chi-square test or Fisher's exact test. Survival analysis was performed using the Kaplan–Meier method with the Log rank test for group comparison. Uni- and multivariate analyses were performed using the Cox proportional hazards model, with results presented as HR and 95% CI. All statistical tests were two-sided, and $P < 0.05$ was considered statistically significant.

All statistical analyses and bioinformatics visualizations were performed using R software (version 4.5.1, R Foundation for Statistical Computing, Vienna, Austria). The analysis was conducted in the Windows 11 environment. Key computational tasks were supported by the "stats" and "base" packages (v4.5.1), and integration was managed via the RStudio interface (v0.17.1).

Results

Baseline Characteristics and SII Stratification

A total of 783 HCC patients were included from the main center in this study, with 535 patients in the surgical cohort and 134 in the immunotherapy cohort. The external center included 114 patients in the surgical cohort. Based on the optimal cutoff value (SII = 374.74) determined from the main center surgical cohort, the overall surgical cohort was divided into low-SII and high-SII groups. The baseline clinical characteristics of each group are shown in Table 1. Kaplan–Meier analysis showed that the RFS of patients in the high-SII group was significantly worse than that in the low-SII group (log-rank $P < 0.0001$) (Figure 2), suggesting a strong correlation between SII and postoperative recurrence risk.

Cox Analysis and Nomogram Construction for High SII Group

In the high-SII patient population, patients were randomly divided into a training cohort (n = 144) and a test cohort (n = 62) at a 7:3 ratio. Univariate Cox regression analysis showed that tumor diameter, Intratumoral Hemorrhage (IH), Satellite Lesions (SL), and gamma-glutamyltransferase (GGT) were significantly associated with RFS (Table 2). Further multivariate Cox regression analysis identified four independent risk factors: tumor diameter HR (Hazard Ratio) = 1.02, 95% CI (Confidence Interval): 1.01–1.03, $P < 0.001$), IH HR (Hazard Ratio) = 1.75, 95% CI (Confidence Interval): 1.01–3.03, $P = 0.047$), SL HR (Hazard Ratio) = 3.56, 95% CI (Confidence Interval): 1.72–7.40, $P < 0.001$), and GGT HR (Hazard Ratio) = 1.01, 95% CI (Confidence Interval): 1.01–1.01, $P < 0.001$). Based on these variables, a nomogram model was constructed to predict 1-, 2-, and 3-year RFS (Figure 3A). The model intuitively demonstrated individualized recurrence risk, the higher the score, the greater the recurrence risk.

Table 1 Baseline Table of Surgical Patients

		Training Cohort (n=535)			Validation Cohort (n=114)		
Variable	**Sort**	**High SII (n=206)**	**Low SII (n=329)**	**p**	**High SII (n=48)**	**Low SII (n=66)**	**p**
IntratumoralFat,n(%)	0	171(83.010)	261(79.331)	0.294	25(52.083)	25(37.879)	0.131
	1	35(16.990)	68(20.669)		23(47.917)	41(62.121)	
IntratumoralHemorrhage,n(%)	0	125(60.680)	238(72.340)	0.005	20(41.667)	20(30.303)	0.209
	1	81(39.320)	91(27.660)		28(58.333)	46(69.697)	
SatelliteLesions,n(%)	0	184(89.320)	297(90.274)	0.722	39(81.250)	57(86.364)	0.46
	1	22(10.680)	32(9.726)		9(18.750)	9(13.636)	
MosaicPattern,n(%)	0	63(30.583)	129(39.210)	0.043	38(79.167)	42(63.636)	0.074
	1	143(69.417)	200(60.790)		10(20.833)	24(36.364)	
IntratumoralCysticDegeneration,n(%)	0	129(62.621)	214(65.046)	0.569	23(47.917)	31(46.970)	0.92
	1	77(37.379)	115(34.954)		25(52.083)	35(53.030)	
PeritumoralEdema,n(%)	0	181(87.864)	302(91.793)	0.135	26(54.167)	28(42.424)	0.215
	1	25(12.136)	27(8.207)		22(45.833)	38(57.576)	
APHE,n(%)	0	7(3.398)	25(7.599)	0.046	26(54.167)	40(60.606)	0.492
	1	199(96.602)	304(92.401)		22(45.833)	26(39.394)	
Washout,n(%)	0	21(10.194)	39(11.854)	0.554	17(35.417)	21(31.818)	0.687
	1	185(89.806)	290(88.146)		31(64.583)	45(68.182)	
Capsule,n(%)	0	24(11.650)	80(24.316)	<0.001	18(37.500)	23(34.848)	0.771
	1	182(88.350)	249(75.684)		30(62.500)	43(65.152)	
CombinedTransientEnhancement,n(%)	0	166(80.583)	274(83.283)	0.426	26(54.167)	36(54.545)	0.968
	1	40(19.417)	55(16.717)		22(45.833)	30(45.455)	
RimlikeEnhancement,n(%)	0	169(82.039)	294(89.362)	0.016	29(60.417)	32(48.485)	0.207
	1	37(17.961)	35(10.638)		19(39.583)	34(51.515)	
NoduleinNodule,n(%)	0	200(97.087)	321(97.568)	0.735	28(58.333)	33(50.000)	0.378
	1	6(2.913)	8(2.432)		20(41.667)	33(50.000)	
IntratumoralIschemia,n(%)	0	114(55.340)	205(62.310)	0.11	28(58.333)	33(50.000)	0.378
	1	92(44.660)	124(37.690)		20(41.667)	33(50.000)	
CombinedDN,n(%)	0	189(91.748)	272(82.675)	0.003	27(56.250)	32(48.485)	0.413
	1	17(8.252)	57(17.325)		21(43.750)	34(51.515)	
SignificantCirrhosis,n(%)	0	68(33.010)	89(27.052)	0.141	40(83.333)	50(75.758)	0.327
	1	138(66.990)	240(72.948)		8(16.667)	16(24.242)	
Ascites,n(%)	0	158(76.699)	262(79.635)	0.421	43(89.583)	56(84.848)	0.46
	1	48(23.301)	67(20.365)		5(10.417)	10(15.152)	

https://doi.org/10.2147/JHC.S588390

Varices,n(%)	0	185(89.806)	291(88.450)	0.626	26(54.167)	28(42.424)	0.215
	1	21(10.194)	38(11.550)		22(45.833)	38(57.576)	
AFP,n(%)	0	140(67.961)	253(76.900)	0.023	44(91.667)	54(81.818)	0.135
	1	66(32.039)	76(23.100)		4(8.333)	12(18.182)	
Diameter,median[IQR]	nan	52.000[33.000,74.000]	40.000[28.000,56.000]	<0.001	51.000[30.000,91.000]	31.000[20.000,48.000]	0.001
AST,median[IQR]	nan	43.000[29.000,87.000]	34.000[24.000,48.000]	<0.001	44.000[22.000,123.000]	31.000[21.000,54.000]	0.042
ALT,median[IQR]	nan	42.000[24.000,83.000]	34.000[21.000,51.000]	<0.001	40.300[18.400,74.000]	27.400[18.200,49.100]	0.127
GGT,median[IQR]	nan	57.000[34.000,101.000]	50.000[29.000,99.000]	0.191	40.000[27.000,82.100]	34.000[24.000,69.000]	0.24
PLT,median[IQR]	nan	183.000[143.000,245.000]	141.000[106.000,172.000]	<0.001	182.000[147.000,222.000]	129.000[98.000,170.000]	<0.001
N,median[IQR]	nan	4.920[3.830,7.060]	2.520[1.960,3.280]	<0.001	4.850[3.600,7.420]	2.170[1.670,2.860]	<0.001
L,median[IQR]	nan	1.290[0.950,1.710]	1.770[1.370,2.220]	<0.001	1.160±0.547	1.521±0.598	0.001
WBC,median[IQR]	nan	7.290[5.810,9.020]	4.950[4.020,6.210]	<0.001	7.080[5.350,9.570]	4.160[3.080,5.280]	<0.001
Hematocrit,median[IQR]	nan	42.100[39.170,45.600]	42.600[39.200,45.200]	0.807	42.800[38.700,45.200]	41.000[37.400,44.400]	0.355
G,median[IQR]	nan	5.000[4.500,6.700]	4.600[4.200,5.300]	<0.001	5.200[4.500,6.400]	4.500[4.000,5.200]	0.002
TotalBilirubin,median[IQR]	nan	13.700[10.310,17.430]	13.800[10.300,17.700]	0.725	17.700[13.300,23.500]	16.200[12.600,21.800]	0.675
DirectBilirubin,median[IQR]	nan	3.500[2.600,5.200]	3.700[2.610,5.600]	0.453	4.900[3.700,6.600]	4.100[3.400,6.200]	0.605
AlkalinePhosphataseALP,median[IQR]	nan	87.000[45.000,120.000]	78.000[40.000,103.000]	0.007	82.000[67.000,112.000]	81.000[69.000,99.000]	0.911
ProthrombinTime,median[IQR]	nan	11.900[11.300,12.700]	12.100[11.500,12.800]	0.119	12.900[12.100,13.600]	12.900[12.300,13.500]	0.527

https://doi.org/10.2147/JHC.S588390

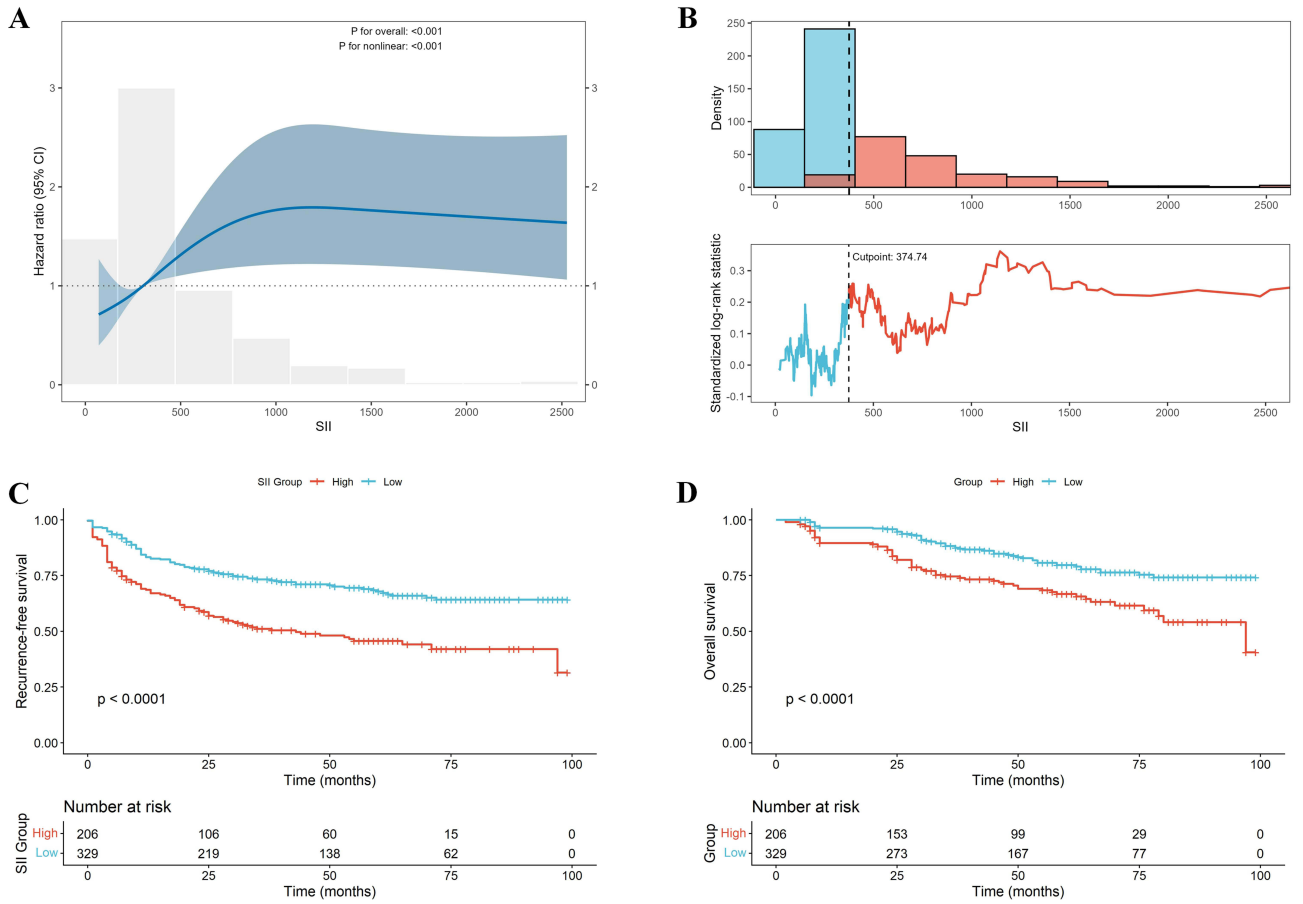

Figure 2 Relationship between SII and prognosis in surgical cohort. (**A**) Restricted cubic spline (Cox model) showed a significant non-linear positive correlation between SII and recurrence risk (overall P< 0.001; nonlinear P < 0.001), 95% CI. (**B**) Determine the optimal cutoff value based on maximally selected log-rank statistics (SII = 374.74); the above image is the SII distribution histogram, and the following image is the standardized log-rank statistic curve. (**C**) RFS Kaplan-Meier curve (log-rank P < 0.0001). (**D**) OS Kaplan-Meier curve (log-rank P < 0.0001).

Model Evaluation and Performance Comparison

The nomogram model showed strong discriminative ability and stability in both the training and test sets. The training set C-index was 0.796, and the test set was 0.775. Time-dependent ROC curves showed that the 1-, 2-, and 3-year AUC for the training set were 0.853, 0.850, and 0.847, respectively, while the internal test set values were 0.836, 0.844, and 0.816 (Figure 3B and C), and the external test set values were 0.74, 0.784, and 0.643 (Figure 3D). Furthermore, a comparative analysis of the nomogram with the AJCC 8th edition and BCLC staging systems (Table 3, Supplementary Figure 1) showed that the C-index of this study's nomogram (training set 0.796, test set 0.775) was significantly higher than that of AJCC (0.663, 0.586) and BCLC (0.644, 0.567) systems in both the training and test sets. The time-dependent ROC analysis also indicated that the nomogram's AUC at the 1-, 2-, and 3-year time points were superior to traditional staging (training set: 0.853, 0.850, 0.847; test set: 0.836, 0.844, 0.816). These results demonstrate that the nomogram based on the high-SII population exhibits higher discrimination and stability in predicting postoperative recurrence risk, outperforming current clinical staging systems.

Risk Stratification and Kaplan–Meier Survival Analysis

Based on the median total nomogram score as the cutoff value, high-SII patients were further divided into high-risk and low-risk groups. Kaplan–Meier curves showed a clear separation in RFS between the two groups: the high-risk group had a significantly higher recurrence rate than the low-risk group (training set log-rank P < 0.0001, internal test set P =

Table 2 Univariate and Multivariate Cox Analysis

Variables	Univariate Analysis					Multivariate Analysis				
	β	S.E	Z	*P*	HR (95% CI)	β	S.E	Z	*P*	HR (95% CI)
IntratumoralFat										
Negative					1.00 (Reference)					
Positive	−0.47	0.36	−1.31	0.189	0.63 (0.31 ~ 1.26)					
IntratumoralHemorrhage										
Negative					1.00 (Reference)					1.00 (Reference)
Positive	0.86	0.24	3.59	<0.001	2.37 (1.48 ~ 3.80)	0.56	0.28	1.98	0.047	1.75 (1.01 ~ 3.03)
SatelliteLesions										
Negative					1.00 (Reference)					1.00 (Reference)
Positive	1.22	0.35	3.44	<0.001	3.37 (1.69 ~ 6.74)	1.27	0.37	3.41	<0.001	3.56 (1.72 ~ 7.40)
MosaicPattern										
Negative					1.00 (Reference)					1.00 (Reference)
Positive	1.17	0.33	3.57	<0.001	3.23 (1.70 ~ 6.16)	0.47	0.37	1.29	0.198	1.60 (0.78 ~ 3.29)
IntratumoralCysticDegeneration										
Negative					1.00 (Reference)					1.00 (Reference)
Positive	0.59	0.24	2.49	0.013	1.80 (1.13 ~ 2.86)	−0.19	0.28	−0.69	0.491	0.82 (0.47 ~ 1.43)
PeritumoralEdema										
Negative					1.00 (Reference)					
Positive	0.44	0.36	1.22	0.224	1.55 (0.77 ~ 3.12)					
APHE										
Negative					1.00 (Reference)					
Positive	−0.98	0.59	−1.65	0.099	0.38 (0.12 ~ 1.20)					
Washout										
Negative					1.00 (Reference)					
Positive	−0.38	0.36	−1.06	0.289	0.68 (0.34 ~ 1.38)					
Capsule										
Negative					1.00 (Reference)					
Positive	0.04	0.38	0.1	0.921	1.04 (0.50 ~ 2.17)					
CombinedTransientEnhancement										
Negative					1.00 (Reference)					
Positive	−0.31	0.33	−0.95	0.344	0.73 (0.39 ~ 1.39)					
RimlikeEnhancement										
Negative					1.00 (Reference)					
Positive	−0.19	0.33	−0.58	0.562	0.83 (0.43 ~ 1.57)					
NoduleinNodule										
Negative					1.00 (Reference)					
Positive	0.19	0.72	0.26	0.796	1.20 (0.29 ~ 4.92)					
IntratumoralIschemia										
Negative					1.00 (Reference)					1.00 (Reference)
Positive	0.84	0.24	3.51	<0.001	2.32 (1.45 ~ 3.72)	−0.06	0.3	−0.21	0.831	0.94 (0.52 ~ 1.69)
CombinedDN										
Negative					1.00 (Reference)					
Positive	−0.37	0.52	−0.71	0.476	0.69 (0.25 ~ 1.90)					
SignificantCirrhosis										
Negative					1.00 (Reference)					
Positive	−0.16	0.24	−0.65	0.515	0.85 (0.53 ~ 1.37)					
Ascites										
Negative					1.00 (Reference)					
Positive	−0.41	0.33	−1.24	0.217	0.67 (0.35 ~ 1.27)					
Varices										
Negative					1.00 (Reference)					
Positive	−0.26	0.47	−0.56	0.576	0.77 (0.31 ~ 1.92)					

(*Continued*)

Table 2 (Continued).

Variables	Univariate Analysis					Multivariate Analysis				
	β	S.E	Z	*P*	HR (95% CI)	β	S.E	Z	*P*	HR (95% CI)
AFP (400)										
Negative					1.00 (Reference)					1.00 (Reference)
Positive	0.74	0.24	3.1	0.002	2.11 (1.32 ~ 3.37)	0.4	0.26	1.56	0.119	1.50 (0.90 ~ 2.49)
Etiology										
Hepatitis B					1.00 (Reference)					
Hepatitis C	−0.03	0.43	−0.08	0.938	0.97 (0.42 ~ 2.24)					
Hepatitis B + C	−0.32	1.01	−0.32	0.751	0.73 (0.10 ~ 5.24)					
Diameter	0.02	0	6.49	<0.001	1.02 (1.02 ~ 1.03)	0.02	0	3.96	<0.001	1.02 (1.01 ~ 1.03)
AST	0	0	0.59	0.552	1.00 (1.00 ~ 1.00)					
ALT	0	0	0.37	0.709	1.00 (1.00 ~ 1.00)					
GGT	0.01	0	5.02	<0.001	1.01 (1.01 ~ 1.01)	0.01	0	3.6	<0.001	1.01 (1.01 ~ 1.01)
WBC	−0.09	0.05	−1.82	0.068	0.91 (0.83 ~ 1.01)					
Hematocrit	−0.01	0.02	−0.29	0.772	0.99 (0.95 ~ 1.04)					
Glucose	−0.02	0.06	−0.31	0.758	0.98 (0.88 ~ 1.10)					
TotalBilirubin	−0.02	0.02	−1.06	0.287	0.98 (0.95 ~ 1.01)					
DirectBilirubin	−0.02	0.05	−0.44	0.66	0.98 (0.89 ~ 1.07)					
AlkalinePhosphatase	0.01	0	2.08	0.038	1.01 (1.01 ~ 1.01)	0	0	1.3	0.192	1.00 (1.00 ~ 1.01)
ProthrombinTime	0.04	0.11	0.32	0.747	1.04 (0.83 ~ 1.29)					

Abbreviations: HR, Hazard Ratio; CI, Confidence Interval.

0.00017, external test set P = 0.033) (Figure 3E–G). This result suggests that the model possesses excellent clinical risk stratification capability.

Validation of the Nomogram in the Immunotherapy Cohort

Patients in the immunotherapy cohort were divided into high-risk and low-risk groups using the median threshold from the surgical cohort training set. Kaplan–Meier curves showed a significant separation in PFS between the two groups (log-rank P = 0.045), with a trend opposite to the surgical cohort: the high-risk group showed markedly better PFS than the low-risk group (Figure 4A). A stacked bar chart further demonstrated that the proportion of disease progression in the low-risk group was significantly higher than in the high-risk group, while the high-risk group had a larger proportion of "no progression" (test P = 0.0356) (Figure 4B). This result suggests that the nomogram, constructed based on the high-SII population, can identify a "high-risk score" subtype that is more likely to benefit from treatment in the immunotherapy setting, demonstrating good cross-scenario risk stratification and efficacy indication value.

Transcriptomic Differences and KEGG Enrichment Analysis

To further explore the molecular differences between risk subgroups in high-SII patients, we conducted transcriptomic analysis on 67 surgical patients with RNA-seq data. Based on the edgeR differential analysis, a total of 779 DEGs were identified, comprising 275 upregulated and 504 downregulated genes (Figure 5A). These DEGs reflect significant transcriptional differences between the high-risk and low-risk groups in immune response and inflammation regulation.

KEGG pathway enrichment analysis (Figure 5B) showed that the DEGs were primarily enriched in immune and inflammation-related pathways, including Cytokine–cytokine receptor interaction, IL-17 signaling pathway, and Rheumatoid arthritis. These pathways are generally involved in immune cell recruitment, inflammatory factor release, and immune signal amplification reactions, suggesting a significant inflammatory activation state within the tumor tissue of high-risk patients.

GO BP enrichment results (Figure 5C) further supported these findings, with significantly enriched terms including humoral immune response, chemotaxis, antimicrobial humoral response, and myeloid leukocyte activation. This indicates

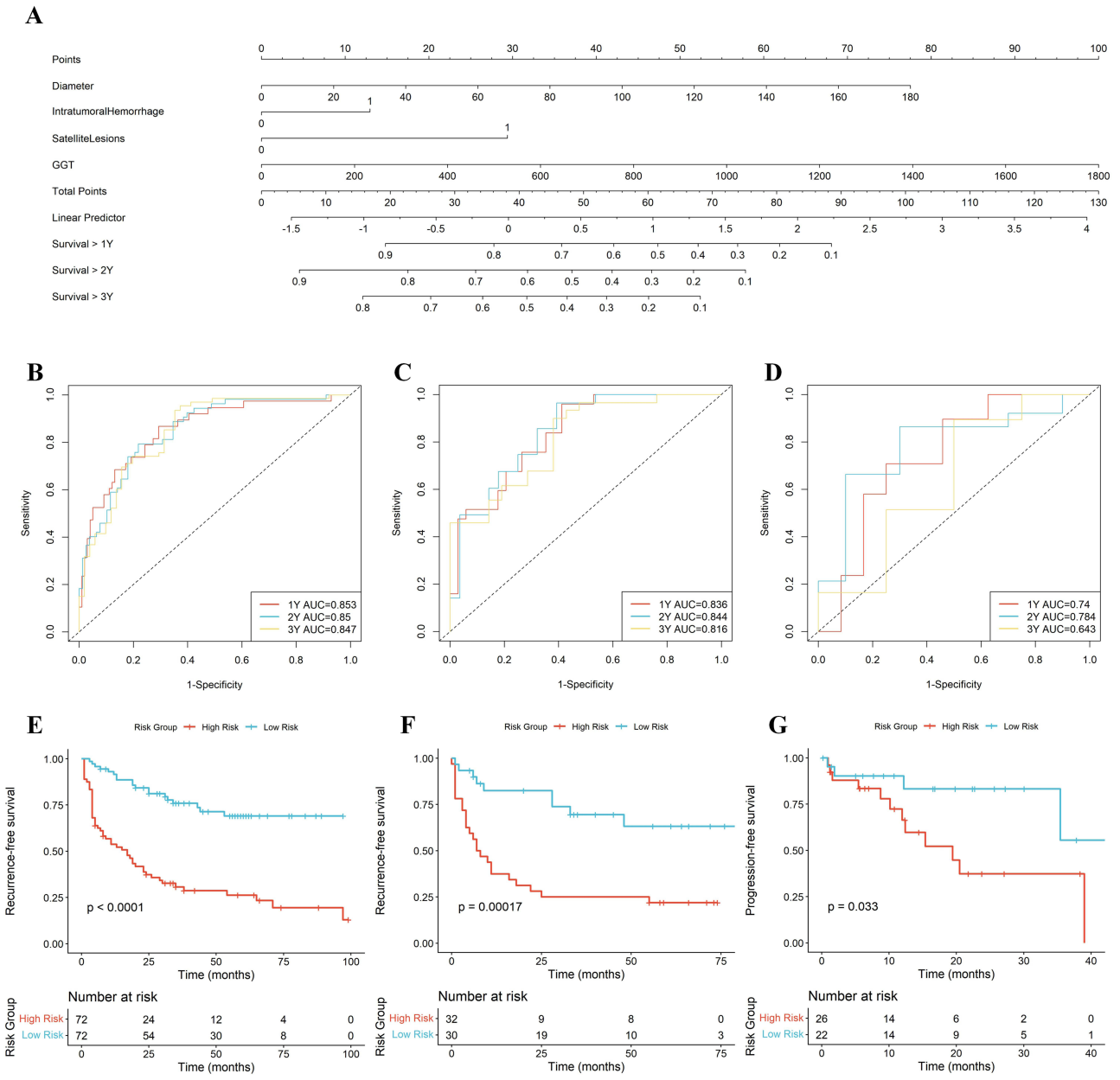

Figure 3 Nomogram of high SII surgery cohort and its performance evaluation. (**A**) A nomogram based on four independent variables (tumor diameter, intratumoral hemorrhage, satellite lesions, GGT). (**B**–**D**) The time-dependent ROC curve of RFS at 1, 2, and 3 years: corresponding to the training set ((**B**): 1Y AUC = 0.853; (**B**–**D**)); 2Y AUC = 0.85; 3Y AUC = 0.847), internal test set ((**C**): 1Y AUC = 0.836; 2Y AUC = 0.844; 3Y AUC = 0.816) and external test set ((**D**): 1Y AUC = 0.740; 2Y AUC = 0.784; 3Y AUC = 0.643). (**E** and **G**) The Kaplan-Meier curve of the high / low risk group in the surgical cohort of patients with high SII, and the RFS of the three cohorts were significantly separated ((**E**): training set, log-rank P < 0.0001; (**F**):internal test set, P = 0.00017; (**G**) external test set, P = 0.033).

that the high-risk group not only has elevated inflammation but may also be accompanied by active innate and adaptive immune responses.

To assess differences in the tumor immune microenvironment, we further employed the CIBERSORT and quanTIseq algorithms to analyze immune cell infiltration between different risk groups. The results showed a significantly higher infiltration level of Regulatory T cells (Tregs)_quantiseq in the high-risk group (Wilcoxon P < 0.05) (Figure 5D). The increase in Tregs suggests enhanced tumor immunosuppression. Notably, the elevated Tregs abundance in the high-risk group was still accompanied by the activation of various inflammation-related signaling pathways, indicating a complex tumor immune microenvironment characterized by "coexistence of immune activation and immunosuppression."

https://doi.org/10.2147/JHC.S588390

Table 3 Comparison of the Efficacy of Nomogram and Traditional Clinical Staging System (AJCC, BCLC)

	Model/Staging System	Performance Measure			
		C-index	Time-Dependent AUC		
			1 Year	2 Year	3 Year
Training cohort	Nomogram	0.796	0.853	0.85	0.847
	AJCC	0.663	0.668	0.628	0.667
	BCLC	0.644	0.635	0.608	0.649
Validation cohort	Nomogram	0.775	0.836	0.844	0.816
	AJCC	0.586	0.52	0.573	0.607
	BCLC	0.567	0.495	0.56	0.567

Drug Sensitivity Analysis

Drug sensitivity analysis, performed using oncoPredict based on the GDSC2 database to predict the half maximal inhibitory concentration (IC_50), showed that high-risk patients were more sensitive to a variety of targeted or DNA repair-related drugs, including Niraparib_1177, Talazoparib_1259, AGI_6780_1634, AZD2014_1441, Wnt_C59_1622, Teniposide_1809, and Obatoclax_Mesylate_1068 (Figure 5E–K). Most of these drugs are associated with PARP inhibition, mTOR pathway, and Wnt signaling inhibition, suggesting that the high-risk group may possess specific molecular vulnerabilities that can be targeted by drugs.

In summary, the DEGs in high-risk patients primarily involve immune-inflammation-related pathways. The tumor microenvironment is characterized by the enrichment of immunosuppressive cells (Tregs) and impaired innate immunity. This transcriptomic profile provides a molecular basis for explaining the adverse prognosis and differential drug response observed in high-SII patients.

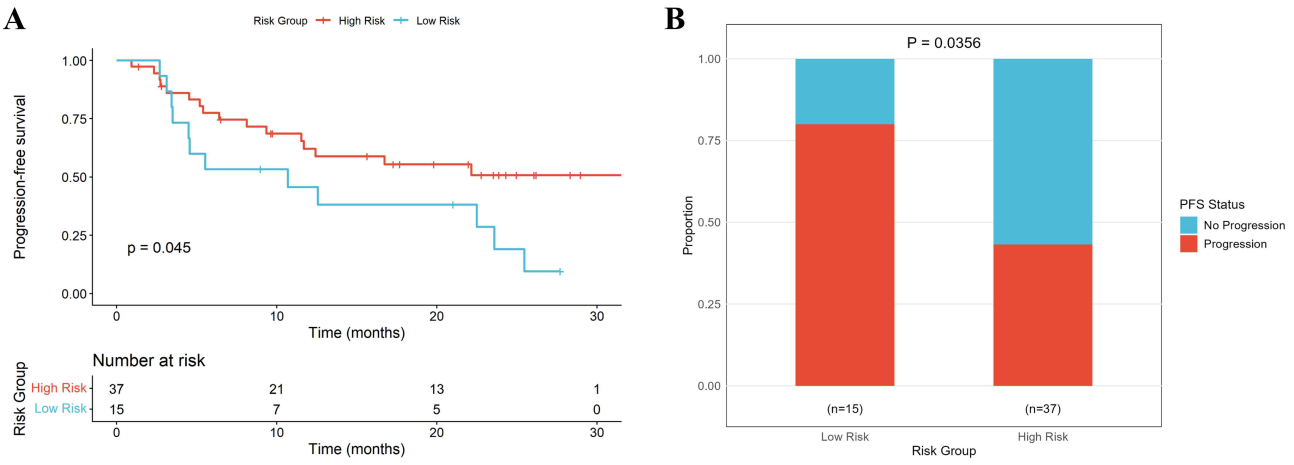

Figure 4 Risk stratification and outcome of immunotherapy cohort (based on median threshold of surgical cohort nomogram). (**A**) Kaplan-Meier curve was used to compare the progression-free survival (PFS) between the high-risk group (red, n = 37) and the low-risk group (blue, n = 15), log-rank P = 0.045. (**B**) Immunotherapy Cohort PFS Progression Status. Stacked column diagram showed the distribution of progression status of the two groups, $\chi 2$ test P = 0.0356.

https://doi.org/10.2147/JHC.S588390

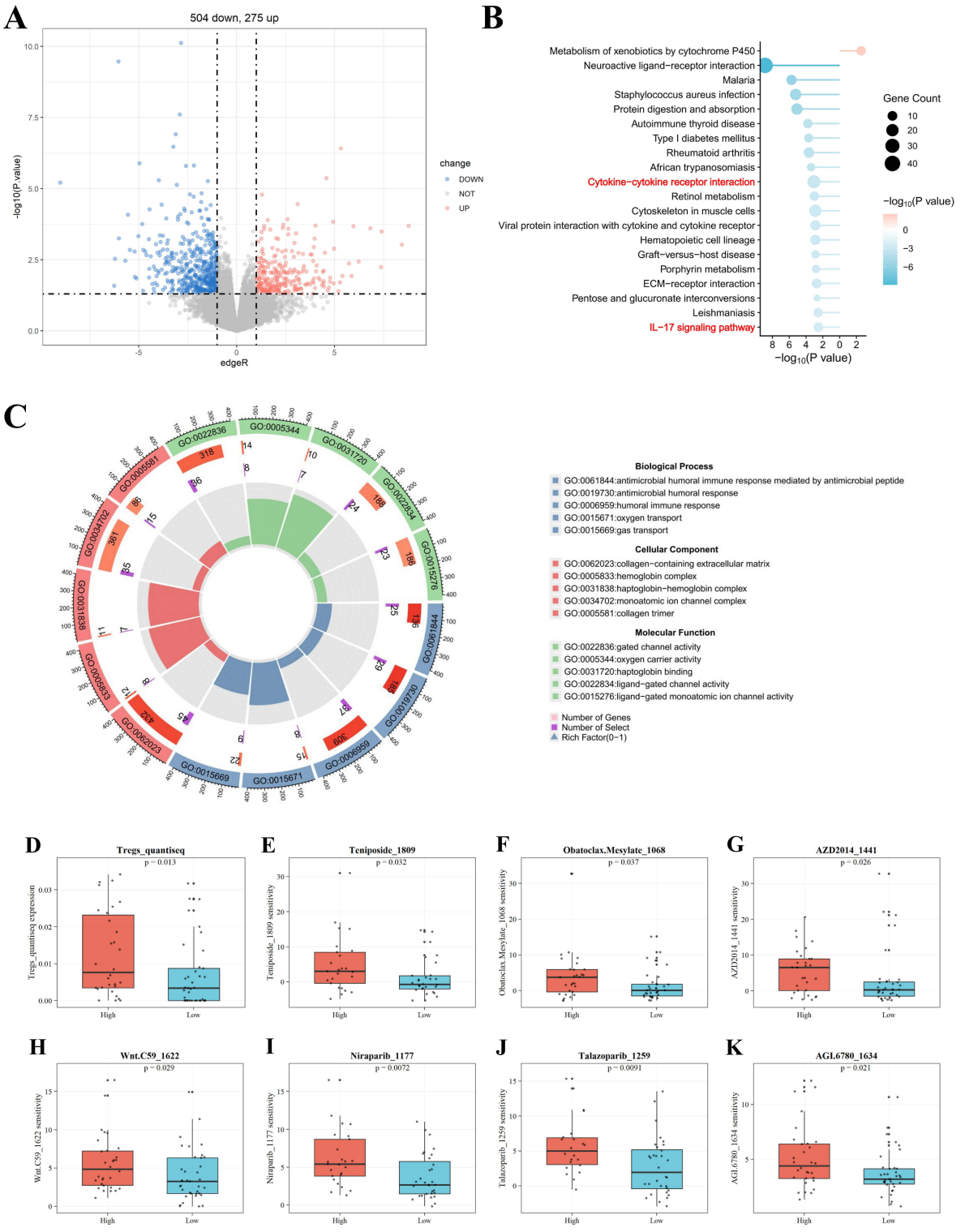

Figure 5 Bioinformatics analysis (high SII surgical cohort, divided into high / low risk groups according to the median of the total score of the nomogram). (**A**) Differentially expressed volcanograms (edgeR, threshold:log $_2$ FC> 1 and FDR < 0.05), a total of 779 DEGs were identified, of which 275 were up-regulated and 504 were down-regulated. (**B**) KEGG enrichment bubble diagram, significant pathways include Cytokine-cytokine receptor interaction, IL-17 signaling pathway, etc. (**C**) GO circle diagram (BP / CC / MF): Enrichment items focused on antibacterial humoral immune response, chemotaxis / migration, myeloid leukocyte activation (BP), hemoglobin complex, monomer / homodimer ion channel complex (CC), oxygen carrier activity, ligand-gated ion channel activity, etc. (MF). (**D**) Immune infiltration analysis (quanTIseq): Tregs - quantiseq infiltration was significantly increased in the high-risk group (Wilcoxon P = 0.013). (**E**–**K**) drug sensitivity analysis (oncoPredict/calcPhenotype based on GDSC2 training): There were significant differences in the predictive sensitivity of the following drugs between the high and low risk groups-Teniposide-1809 (P = 0.032), Obatoclax-Mesylate-1068 (P = 0.037), AZD2014-1441 (P = 0.035), Wnt-C59-1622 (P = 0.057), Niraparib-1177 (P = 0.072), Talazoparib-1259 (P = 0.029) and AGI-6780-1634 (P = 0.031).

https://doi.org/10.2147/JHC.S588390

Discussion

This study identified the SII as a key biomarker for stratifying HCC patients and developed an individualized prognostic model integrating radiological and biochemical indicators, specifically designed for populations with a high inflammatory burden. The nomogram, constructed based on four independent prognostic factors—TD, IH, SL, and GGT—effectively predicted 1-, 2-, and 3-year RFS after surgery. Notably, the model demonstrated not only excellent performance in postoperative recurrence prediction but also potential translational value in the IO cohort. High-risk patients identified by the nomogram achieved better PFS following ICI therapy, suggesting that inflammation-driven tumor biology may influence therapeutic sensitivity by reshaping the IME. Compared with traditional staging systems or single inflammatory indices, the present strategy more comprehensively reflects the interplay between inflammation and immunity, enabling more precise risk stratification and identification of patients who may benefit from IO. Overall, the proposed nomogram serves as a reliable tool for postoperative prognostic assessment while bridging inflammatory status with immune responsiveness, offering a novel conceptual framework for precision management of HCC patients with high SII.

SII, as a composite index integrating platelet, neutrophil, and lymphocyte counts, comprehensively reflects the body's inflammatory response and immune status.[11,13] Elevated platelet and neutrophil counts suggest pro-angiogenic and pro-tumor inflammatory responses, while lymphopenia indicates decreased anti-tumor immunity. Together, these three components form a "state of inflammatory immune imbalance" associated with poor prognosis. Multiple studies have reported SII as an independent risk factor for HCC, significantly associated with OS and DFS/RFS.[11] However, most previous studies used SII as a continuous variable or simple stratification. This study, by focusing on the high-SII high-risk subpopulation based on the optimal SII cutoff, better reflects the prognostic heterogeneity of the "high inflammatory burden" population and enhances the model's clinical utility.

Radiological features such as tumor diameter, IH, and SL are all closely associated with local invasiveness and microvascular invasion of the tumor, serving as important radiological signals for HCC recurrence and metastasis.[14–16] This study integrated these features with GGT, an indicator reflecting intrahepatic cholestasis and oxidative stress levels,[15] into the nomogram model. This approach not only compensates for the shortcomings of relying solely on hematological indicators to reflect tumor biological behavior but also makes the model more representative in characterizing the "radiology-inflammation-immune" interaction. In contrast, traditional staging systems (such as AJCC and BCLC) are primarily based on tumor burden and liver function status, failing to fully reflect the host's immune-inflammatory level and its regulation of tumor behavior. While traditional systems often overlook the systemic inflammatory milieu, our results (Table 3 and Supplementary Figure 1) demonstrate that the nomogram significantly outperforms AJCC and BCLC in both discriminative ability and stability across training and validation sets. This suggests that combining inflammatory biomarkers (SII, GGT) with radiological invasive features (tumor diameter, hemorrhage, SL) can effectively improve the accuracy and generalization performance of the model in predicting postoperative recurrence risk, offering clinicians a simple, operable risk assessment tool that is more individualized than traditional staging systems.

ICIs therapy has become a vital component of HCC treatment.[17–19] When the established model from this study was migrated to the immunotherapy cohort, a significant "reversal phenomenon" was observed: the high-risk group patients, predicted to have the highest recurrence risk in the high-SII surgical population, exhibited better PFS in the immunotherapy setting. This phenomenon suggests that, within the high-SII population, the high-risk subgroup defined by the nomogram—characterized by larger tumor size, the presence of SL, IH, and elevated serum GGT—is not merely a group with poor prognosis, but may represent an immunologically plastic tumor phenotype. In the absence of exogenous immune stimulation, this phenotype is driven toward recurrence by a combination of high inflammatory burden, metabolic stress, and local invasiveness. However, under the action of ICIs, it may be "reprogrammed" due to the high activation level of inflammation-immune pathways, thereby exhibiting a stronger immune response capacity.

From a biological perspective, this "prognostic reversal" phenomenon has a rational immunological basis. Transcriptomic analysis revealed that the DEGs in high-risk patients were significantly enriched in the Cytokine–cytokine receptor interaction and IL-17 signaling pathway, which together drive immune cell recruitment and the amplification cascade of pro-inflammatory cytokines. On one hand, this inflammatory amplification might promote

tumor residue, angiogenesis, and immune escape in the postoperative setting, leading to increased recurrence risk. On the other hand, in the immunotherapy environment, this pre-activated inflammatory state provides a favorable "fuel" for immune rebooting. Specifically, increased tumor diameter and the presence of SL suggest more microvascular invasion and necrotic areas, which promote antigen release and chemokine production.[20–23] IH accompanied by ischemia–reperfusion injury can enhance immunogenic cell death signals.[24] Furthermore, elevated GGT, representing oxidative-reductive stress and glutathione metabolism imbalance, may act as a metabolic driver for the immune response.[25,26] These features collectively shape a complex microenvironment that is both immune-activated and immunosuppressive, which can be redirected toward anti-tumor immunity after the intervention of immune blockade signals.

This characteristic is highly consistent with the recently proposed "Inflamed Immune Phenotype." Montironi et al[27] classified the HCC immune landscape into "hot" and "cold" phenotypes through multi-omics studies. The former is characterized by higher Interferon-gamma (IFN-γ) signaling, cytotoxic gene expression, and immune infiltration, and is significantly associated with ICIs response. Chen and Mellman[28] proposed the "Cancer–Immune Set Point" theory, further suggesting that the balance among host inflammation status, the degree of tumor immune activation, and microenvironment inhibitory signals determines the threshold for immunotherapy response. Within this framework, the "SII + high-risk features" patients identified in this study can be viewed as a subpopulation with a lower immune set point, easily activated by exogenous blockade. Spatial transcriptomics studies also show that the immune barrier composed of SPP1^+ macrophages and Cancer-Associated Fibroblasts (CAFs) at the tumor boundary is a critical structure limiting T cell (T cell) infiltration. However, in some "HOT" phenotype samples, this barrier can be reshaped by inflammatory signals and ICIs treatment, thereby restoring immune cell entry and enhancing response.[29]

Additionally, our drug sensitivity analysis suggested that high-risk patients were more sensitive to drugs like PARP inhibitors (Niraparib, Talazoparib), mTOR inhibitors (AZD2014), and Wnt pathway inhibitors. This phenomenon may be related to inflammation-driven activation of DNA repair pathways and metabolic stress, supporting recent research on "inflammation–DNA damage response interaction" and "metabolism–immune co-regulation".[30] These molecular features indicate that the high-risk subtype not only possesses an inflammatory microenvironment that can be immunologically reprogrammed but also has metabolic vulnerabilities that can be targeted, providing new biological evidence for combination immuno-targeted therapy.

In summary, SII is not only an inflammatory biomarker for postoperative recurrence risk in HCC but also reflects a state of immune plasticity in the tumor. When immune intervention is absent, the high inflammatory and highly invasive features of this state synergistically drive recurrence. However, in the context of immunotherapy, this state is reshaped into an immune-activated microenvironment, resulting in a shift from poor prognosis to therapeutic benefit. This finding offers a new perspective on understanding the dual role and plasticity of the inflammation-immune axis and suggests that SII-derived models can be used to identify high-risk populations more likely to benefit from ICIs therapy, providing a basis for formulating individualized treatment strategies.

The innovations of this study, compared to previous research, include: (1) Focusing on the high-SII subpopulation, revealing the clinical heterogeneity of this special immune-inflammatory phenotype; (2) Constructing a concise nomogram integrating radiological invasive features (IH, SL) and GGT, balancing predictive power with generalizability; (3) The first validation of the cross-scenario migratory capability of an SII-derived model in an immunotherapy cohort; (4) Molecular explanation of the immunological basis for the "high-risk group unexpectedly benefiting" phenomenon through transcriptomic and immune microenvironment analyses. Overall, this study not only expands the application boundaries of SII in HCC risk assessment but also provides new theoretical evidence and clinical insights for exploring the association between the inflammation-immune axis and immunotherapy response.

Limitation

Despite the promising findings, several limitations of this study should be acknowledged. First, although this is a multi-center study, its retrospective nature means that potential selection bias could still exist. Future prospective trials are needed to further validate the clinical utility of the nomogram. Second, while our model demonstrated predictive value in the immunotherapy cohort, the sample size for this specific subgroup remains relatively small. Larger-scale cohorts are

necessary to further confirm the robust performance and generalizability of the model across diverse immunotherapy regimens.

Conclusion

In conclusion, this study focused on the HCC population with a high inflammatory burden and developed a robust, non-invasive nomogram integrating radiological and biochemical features. Our findings suggest that this model can accurately predict postoperative RFS and effectively identify patient cohorts more likely to benefit from immunotherapy. By bridging inflammatory status with immune responsiveness through transcriptomic insights, this study provides a promising framework for the precision management and individualized therapeutic decision-making in HCC patients with high SII.

Informed Consent

This retrospective study was approved by the Ethics Committee of Harbin Medical University Cancer Hospital (Approval No. KY-2024-33). The committee waived the requirement for informed consent in view of the retrospective nature of the research and because it did not impactimpact on the clinical care of the patients involved. All procedures performed in the study were in strict adherence to the ethical standards outlined in the Declaration of Helsinki and its subsequent amendments.

Acknowledgments

The authors would like to thank all the clinicians, patients, and staff from the participating centers for their support and contributions to this study. The authors also acknowledge the support from the Climbing Program of Harbin Medical University Cancer Hospital (PDYS2024-10), the Teaching Reform Project of the Third Clinical College of Harbin Medical University (JXZX240021), the Research Fund of Harbin Medical University Cancer Hospital (JS2024-25), the National Natural Science Foundation of China (No. 82572191) and Natural Science Foundation of Heilongjiang Province (PL2024H186).

Author Contributions

All authors made a significant contribution to the work reported, whether that is in the conception, study design, execution, acquisition of data, analysis and interpretation, or in all these areas; took part in drafting, revising or critically reviewing the article; gave final approval of the version to be published; have agreed on the journal to which the article has been submitted; and agree to be accountable for all aspects of the work.

Funding

This work was supported by the Climbing Program of Harbin Medical University Cancer Hospital (PDYS2024-10), the Teaching Reform Project of the Third Clinical College of Harbin Medical University (JXZX240021), the Research Fund of Harbin Medical University Cancer Hospital (JS2024-25), the National Natural Science Foundation of China (No. 82572191) and Natural Science Foundation of Heilongjiang Province (PL2024H186).

Disclosure

The authors declare that they have no conflicts of interest to disclose.

References

1. Koshy A. Evolving global etiology of hepatocellular carcinoma (HCC): insights and trends for 2024. *J Clin Exp Hepatol*. 2025;15(1):102406. doi:10.1016/j.jceh.2024.102406
2. Maki H, Hasegawa K. Advances in the surgical treatment of liver cancer. *Biosci Trends*. 2022;16(3):178–188. doi:10.5582/bst.2022.01245
3. Sugawara Y, Hibi T. Surgical treatment of hepatocellular carcinoma. *Biosci Trends*. 2021;15(3):138–141. doi:10.5582/bst.2021.01094
4. Donne R, Lujambio A. The liver cancer immune microenvironment: therapeutic implications for hepatocellular carcinoma. *Hepatology*. 2023;77(5):1773–1796. doi:10.1002/hep.32740

5. Huang A, Yang XR, Chung WY, Dennison AR, Zhou J. Targeted therapy for hepatocellular carcinoma. *Signal Transduct Target Ther*. 2020;5(1):146. doi:10.1038/s41392-020-00264-x
6. Rimassa L, Finn RS, Sangro B. Combination immunotherapy for hepatocellular carcinoma. *J Hepatol*. 2023;79(2):506–515. doi:10.1016/j.jhep.2023.03.003
7. Oura K, Morishita A, Tani J, Masaki T. Tumor immune microenvironment and immunosuppressive therapy in hepatocellular carcinoma: a review. *Int J Mol Sci*. 2021;22(11):5801. doi:10.3390/ijms22115801
8. Wang Z, Wang Y, Gao P, Ding J. Immune checkpoint inhibitor resistance in hepatocellular carcinoma. *Cancer Lett*. 2023;555:216038. doi:10.1016/j.canlet.2022.216038
9. Song Y, Guo W, Li Z, Guo D, Li Z, Li Y. Systemic immune-inflammation index is associated with hepatic steatosis: evidence from NHANES 2015-2018. *Front Immunol*. 2022;13:1058779. doi:10.3389/fimmu.2022.1058779
10. Xie R, Xiao M, Li L, et al. Association between SII and hepatic steatosis and liver fibrosis: a population-based study. *Front Immunol*. 2022;13:925690. doi:10.3389/fimmu.2022.925690
11. Hu B, Yang XR, Xu Y, et al. Systemic immune-inflammation index predicts prognosis of patients after curative resection for hepatocellular carcinoma. *Clin Cancer Res*. 2014;20(23):6212–6222. doi:10.1158/1078-0432.Ccr-14-0442
12. Zhou Y, Dai M, Zhang Z. Prognostic significance of the systemic immune-inflammation index (SII) in patients with small cell lung cancer: a meta-analysis. *Front Oncol*. 2022;12:814727. doi:10.3389/fonc.2022.814727
13. Wang RH, Wen WX, Jiang ZP, et al. The clinical value of neutrophil-to-lymphocyte ratio (NLR), systemic immune-inflammation index (SII), platelet-to-lymphocyte ratio (PLR) and systemic inflammation response index (SIRI) for predicting the occurrence and severity of pneumonia in patients with intracerebral hemorrhage. *Front Immunol*. 2023;14:1115031. doi:10.3389/fimmu.2023.1115031
14. Carr BI, Guerra V, Giannini EG, et al. Significance of platelet and AFP levels and liver function parameters for HCC size and survival. *Int J Biol Markers*. 2014;29(3):e215–23. doi:10.5301/jbm.5000064
15. Yang Z, Ye P, Xu Q, et al. Elevation of serum GGT and LDH levels, together with higher BCLC staging are associated with poor overall survival from hepatocellular carcinoma: a retrospective analysis. *Discov Med*. 2015;19(107):409–418.
16. Liu L, Qin S, Lin K, et al. Development and comprehensive validation of a predictive prognosis model for very early HCC recurrence within one year after curative resection: a multicenter cohort study. *Int J Surg*. 2024;110(6):3401–3411. doi:10.1097/js9.0000000000001467
17. Shen KY, Zhu Y, Xie SZ, Qin LX. Immunosuppressive tumor microenvironment and immunotherapy of hepatocellular carcinoma: current status and prospectives. *J Hematol Oncol*. 2024;17(1):25. doi:10.1186/s13045-024-01549-2
18. Llovet JM, Castet F, Heikenwalder M, et al. Immunotherapies for hepatocellular carcinoma. *Nat Rev Clin Oncol*. 2022;19(3):151–172. doi:10.1038/s41571-021-00573-2
19. Sangro B, Sarobe P, Hervás-Stubbs S, Melero I. Advances in immunotherapy for hepatocellular carcinoma. *Nat Rev Gastroenterol Hepatol*. 2021;18(8):525–543. doi:10.1038/s41575-021-00438-0
20. Li C, Ouyang W, Yang T. The association of microvascular invasion with satellite nodule, tumor multiplicity, tumor encapsulation and resection margin of hepatocellular carcinoma. *J Hepatol*. 2022;77(3):890–891. doi:10.1016/j.jhep.2022.03.036
21. Gupta T, Jarpula NS. Hepatocellular carcinoma immune microenvironment and check point inhibitors-current status. *World J Hepatol*. 2024;16(3):353–365. doi:10.4254/wjh.v16.i3.353
22. Ruishi X, Linyi X, Yunfan B, et al. New perspectives on chemokines in hepatocellular carcinoma therapy: a critical pathway for natural products regulation of the tumor microenvironment. *Front Immunol*. 2024;15:1456405. doi:10.3389/fimmu.2024.1456405
23. Wang W, Guo Y, Zhong J, et al. The clinical significance of microvascular invasion in the surgical planning and postoperative sequential treatment in hepatocellular carcinoma. *Sci Rep*. 2021;11(1):2415. doi:10.1038/s41598-021-82058-x
24. Lu K, Li H, Sun L, et al. Comprehensive analysis of immunogenic cell death-related genes in liver ischemia-reperfusion injury. *Front Immunol*. 2025;16:1545185. doi:10.3389/fimmu.2025.1545185
25. Moriwaki S, Into T, Suzuki K, et al. γ-Glutamyltranspeptidase is an endogenous activator of Toll-like receptor 4-mediated osteoclastogenesis. *Sci Rep*. 2016;6:35930. doi:10.1038/srep35930
26. Strasak AM, Rapp K, Brant LJ, et al. Association of gamma-glutamyltransferase and risk of cancer incidence in men: a prospective study. *Cancer Res*. 2008;68(10):3970–3977. doi:10.1158/0008-5472.Can-07-6686
27. Montironi C, Castet F, Haber PK, et al. Inflamed and non-inflamed classes of HCC: a revised immunogenomic classification. *Gut*. 2023;72(1):129–140. doi:10.1136/gutjnl-2021-325918
28. Chen DS, Mellman I. Elements of cancer immunity and the cancer-immune set point. *Nature*. 2017;541:7637):321–330. doi:10.1038/nature21349
29. Liu Y, Xun Z, Ma K, et al. Identification of a tumour immune barrier in the HCC microenvironment that determines the efficacy of immunotherapy. *J Hepatol*. 2023;78(4):770–782. doi:10.1016/j.jhep.2023.01.011
30. Greten TF, Villanueva A, Korangy F, et al. Biomarkers for immunotherapy of hepatocellular carcinoma. *Nat Rev Clin Oncol*. 2023;20(11):780–798. doi:10.1038/s41571-023-00816-4